Supplementary Information — Organization of ice multiplication mechanisms among basic cloud types. Part I: Control simulations

Akash Deshmukh[1,2*], Deepak Waman[1,3], Ashok Kumar Gupta[4], Martanda Gautam[1,5], Vaughan Phillips[1*], Aaron Bansemer[6], Paul Connolly[7], Greg McFarquhar[8], Paul J. DeMott[9], Jiwen Fan[10], Yun Lin[11], Jann Schrod[12], Heinz Bingemer[12]

[1]Department of Physical Geography and Ecosystem Science, University of Lund, Lund, Sweden.
[2]University of Lille, CNRS, UMR 8518 - LOA - Laboratoire d'Optique Atmospherique, Lille, France.
[3]Currently at Institute of Meteorology and Climate Research Troposphere Research, Karlsruhe Institute of Technology, Karlsruhe, Germany, Karlsruhe, Germany.
[4]Department of Earth and Environmental Sciences, Vanderbilt University, Nashville, Tennessee, USA.
[5]Currently at Johannes Gutenberg University, Mainz, Germany.
[6]Mesoscale and Microscale Meteorology Laboratory, National Center for Atmospheric Research, Boulder, Colorado, USA.
[7]Department of Earth and Environmental Sciences and Cooperative Institute for Severe and High Impact Weather Research and Operations, The University of Manchester, Manchester, UK.
[8]School of Meteorology and Cooperative Institute for Severe and High Impact Weather Research and Operations, University of Oklahoma, Norman, OK, USA.
[9]Department of Atmospheric Science, Colorado State University, CO, USA.
[10]Environmental Science Division, Argonne National Laboratory, IL, USA.
[11]Joint Institute for Regional Earth System Science and Engineering, University of California, Los Angeles, Los Angeles, CA, USA.
[12]Institute for Atmospheric and Environmental Sciences, Goethe-University, Frankfurt, Germany.

*Corresponding author(s). E-mail(s): akash.deshmukh@univ-lille.fr;
vaughan.phillips@mgeo.lu.se;

Content:
S1 Representation of Secondary Ice Production Mechanisms in AC;
S2 Initialization of Aerosol Loadings in AC;
S3 AC Model validation;
S4 Supplementary Figures

S1 Representation of Secondary Ice Production Mechanisms in AC

SIP is an outcome of microphysical processes, classically involving the fragmentation of pre-existing precipitation particles in clouds. Pre-existing ice (primary ice) may initiate from the ice nucleation either homogeneously or heterogeneously. SIP mechanisms are critical to predict the ice concentration appropriately in natural clouds Hobbs [1], Hobbs et al. [2], Pruppacher and Klett [3]. Secondary ice can emerge due to rime splintering, collision fragmentation, raindrop-freezing by various mechanisms [4, 5] and sublimation fragmentation [6]. In the AC, the following four SIP mechanisms are present and the remaining mechanisms are not present. The representation of these SIP mechanisms in AC is described as follows:

1. **HM process of rime splintering**

Ice splintering is associated with the riming of ice particles. Graupel and hail are rimed and consequently dense. The HM process includes ice particles splintering in the range of temperatures from -3^{o} to -8^{o}C. The HM process requires a broad spectrum of in-cloud droplets bigger than 24 μm with an impact speed of at least 0.2 m/s in this temperature range [4]. These dependencies are represented by simple empirical functions of temperature and mean droplet size.

2. **Ice-ice collision fragmentation**

Ice particles tend to fragment when they collide and form secondary ice. Vardiman [7] experimentally observed that ice-ice collisions should produce splinters in natural clouds. Initial model implementations were pioneered for crystal-crystal collisions in Arctic cloud simulations [8] and theoretically for collisions involving graupel [9]. Phillips et al. [10] created a comprehensive scheme of fragmentation in ice-ice collisions connecting various microphysical species, such as crystals, snow, graupel and hail. They used a theoretical basis relating numbers of fragments to initial kinetic energy and attuned it to observations by Vardiman [7] and Takahashi and Nagao [11]. This scheme has been updated in light of observations of snow outdoors in northern Sweden [12].

3. **Raindrop-freezing fragmentation**

Fragmentation of freezing raindrops or drizzle is another mechanism of ice multiplication, which has been partially seen in several laboratory tests since the 1960s[13–16].

An empirical formulation was designed for all-natural sizes of rain/drizzle and for all subzero temperatures in the mixed-phase region, using data for drops in free-fall from published lab experiments [5]. None of the published observations of electrodynamically levitated drops were used. Phillips et al. [5] came up with two modes of fragmentation in the course of a collision of massive drops and ice particles (mode 1) and a collision of raindrops and massive ice particles (mode 2). Regarding Mode 1, the occurrence of raindrop-freezing fragmentation in mode 1 is more limited at temperatures away from the optimum near -15°C or if drops are tiny (e.g., drop size smaller

than 0.1 mm). Ice enhancement ratios of up to 100-1000 are possible, according to their bin model and 0D theory. However, in mode 2, raindrop-freezing fragmentation is more consequential over a wider range of freezing temperatures, even well away from $-15°C$ than for mode 1. Also, mode 2 is acutely sensitive to the size of the drop.

4. **Sublimational fragmentation**

Fragmentation during sublimation of ice has been observed by Schaefer and Cheng [17], Oraltay and Hallett [18] and Bacon et al. [19]. These laboratory experiments have involved the observations of single ice particles for several temperatures and subsaturated humidities with respect to ice. For example, Oraltay and Hallett [18] observed fragmentation due to the sublimation of dendritic crystals. In the same way, Bacon et al. [19] looked into the fragmentation of frost-levitated particles and Dong et al. [20] observed the fragmentation of rimed particles with different densities.

An empirical formulation was established by Deshmukh et al. [6] based on laboratory experiments and implemented in AC. It accurately captures the sublimational breakup behavior of graupel and dendritic snow particles by considering several influential factors, such as particle size, temperature, and sublimation rate. The formulation was developed based on the observational dataset of laboratory experiments, enhancing its reliability and formulation applicability. A theoretical scaling analysis of a weak deep convective downdraft of 2 m/s and an initial population of 3 L^{-1} and 2 mm monodisperse dendritic snow and graupel particles yields an estimated ice enhancement ratio of roughly 5 and 10, respectively.

S2 Initialization of Aerosol Loadings in AC

The aerosol loadings for all simulated clouds are given in Table S1. For the initialization of loadings in the model, the ground-based observations of aerosol species (e.g., ammonium sulfate, mineral dust, sea salt, soot and total organic carbon) are used to alter the profile from Goddard Chemistry Aerosol Radiation and Transport (GOCART) model [21].

S2.1 ACAPEX

The ground-based measurement of aerosols is done by Integration Monitoring of Protected Visual Environments (IMPROVE) network. The Bliss (named 'Bliss SP') and Lake Tahoe Community College (named 'LTCC1') measurement stations are near to the simulation domain. The observations are averaged over 5 to 11th February 2015 to minimize the error in the aerosol concentrations. The fraction of soot surface area from fossil-fuel combustion (F_OC in the empirical parameterization of INP activity by Phillips et al. [22]) is assumed to be 0.5 parsimoniously, since the westerly flow over the Pacific Ocean reaching the observational area originates from regions of Asia where there is biomass burning at that time of year (e.g., Northern India in Winter after the crop harvest) and the usual industrial/urban pollution.

Species of aerosols				Aerosol Concentrations (μg m^{-3})			
				ACAPEX	STEPS	MC3E	GOAmazon
Sea salt				0.02	0.05	0.061	0.03
Ammonium sulfate ($(NH_4)_2SO_4$)				0.18	1.256	0.71	0.23
Mineral Dust				0.030	0.919	0.175	0.4
Black carbon or soot				0.015	0.034	0.25	0.3
Total Organic Carbon	Soluble organic carbon (80% of total organic carbon)			0.28	1.17	1.38	0.048
	Insoluble organic carbon (20% of total organic carbon)	50% Insoluble organic carbon		0.011	0.177	0.173	0.012
		50% primary biological aerosol particles (PBAP's)	Fungi	0.0041	0.07	0.067	3.92×10^{-3}
			Bacteria	0.00139	0.023	0.0225	1.30×10^{-3}
			Pollen	0.00182	0.055	0.054	3.11×10^{-3}
			Detritus	0.0034	0.03	0.029	1.70×10^{-3}
			Algae	2.69×10^{-6}	4.45×10^{-5}	4.33×10^{-5}	2.51×10^{-6}

Table S1 Aerosol concentrations by species across four measurement campaigns.

S2.2 STEPS

Aerosol measurements were not taken as part of the STEPS campaign. Aerosol loadings, on the other hand, were monitored at neighboring stations by IMPROVE sites. Profiles of mass concentration (2.5µm diameter particles) were scaled at all levels to match IMPROVE averaged observations from the White River (3.4 km MSL) and Great Sand Dunes (2.5 km MSL) sites in Colorado. All concentrations of aerosol species are given in Table S1. In the STEPS campaign, there are no observational data for CCN.

S2.3 MC3E

The detailed initialization and aerosol loadings are given by Waman et al. [23]. The aerosol loadings can be found in Table S1.

S2.4 GOAmazon

The values of aerosol mass mixing ratio for sulphate, dust and organic carbon are from averaged output of Model for OZone and Related chemical Tracers (MOZART) for the day after that simulated. This average is fed to GOCART to generate the aerosol profile for initialization of AC. The remaining species of black carbon and sodium chloride are taken from the observational sites of GOAmazon, located at Manacapuru, Amazonia, Brazil. The data was collected for every 5 minutes on 19th March 2014. The data is averaged for a day to get aerosol loadings (Table S1). The fraction of soot surface area from fossil-fuel combustion (F_OC from Phillips et al. [22]) is assumed to be 0.9 because there is little biomass burning in the forest during the wet season while there is a plume of industrial/urban pollution continually downwind from Manaus in the simulated area (remote sources of biomass burning). The Amazon Basin displays variations in space and time regarding the types and concentrations of aerosol particles. However, there is no influence of pollution from nearby or faraway sources, particularly during the rainy season; the Amazon region has one of the lowest levels of aerosol concentration among all continental regions [24, 25]). This aerosol conditions referred as “green ocean” aerosols [26].

S3 AC Model validation

The control simulations of all four campaign cases are compared with co-incident observations for various dynamical and microphysical quantities from aircraft and ground-based measurements. In the simulations, all SIP mechanisms below *Sec.* S1 are active.

Figure S1ab shows, for the ACAPEX case, the CCN and INP activity spectra predicted by AC and observed. The comparison is performed by stopping the model just outside clouds at the start and predicting CCN/INP activity spectra at the observed level using the activation scheme with simulated aerosol properties. Supersaturation is prescribed over a representative range, allowing spectra to be predicted as a function of supersaturation consistent with observations. There is adequate agreement in view

of the variability of the measurements (Fig. S1ab). The CCN activity spectrum measurements are from the CCN counter mounted on the research vessel Ron Brown. INP measurements were from the G-1 aircraft, flying over coastal to mountain regions [27]. For ACAPEX, INP activity was measured using a continuous flow diffusion chamber (CFDC), sampling outside clouds (isokinetic inlet) and inside clouds (counterflow virtual impactor). Data, averaged at selected temperatures, primarily represent immersion freezing under controlled supersaturation (5−8%) and temperatures (−20 to −30 °C). Optical detection and background checks ensured robust measurements.

Figure S1c shows the validation of the CCN activity spectrum predicted and observed for the GOAmazon case. CCN measurements for the GOAmazon case are from the CCN counter of the observation facility in Manacapuru, Amazonia. The ground-based INP measurements are from the Amazon Tall Tower Observatory (ATTO), (2.144 °S, 59.000 °W, ˜80 m MSL), [28]. The predicted CCN spectra (e.g., 500 CCN cm^{-3} at 1% supersaturation) exhibited reasonable agreement to within 20% of mean values observed at the T3 site (3.2133 °S, 60.5987 °W) in view of measurement uncertainties. These observations were obtained from the ARM Mobile Aerosol Observing System (MAOS), operating approximately 10 m above ground level.

Active INP measurements are not available for GOAmazon, so the prediction is compared with observations from the same month a year later at ATTO (Fig. S1d), which is 150 km northeast of Manaus. Measurements at the ATTO site are available for specific time periods from March to May 2016. Sampling was conducted at local noon for about 1 hour each session, with a frequency of one sample every two days. The samples were analyzed using the FRIDGE (FRankfurt Ice Nuclei Deposition FreezinG Experiment) INP counter. Measurements were taken at temperatures of −20 °C, −25 °C, and −30 °C, with relative humidities close to water saturation, inside the counter. The instrument targets the deposition and condensation modes of INP activity [28].

For STEPS, validation of predicted CCN spectra was shown by Phillips et al. [29], but no INP observations were available in that campaign for direct comparison. For MC3E, both predicted CCN and INP activity spectra were evaluated by [30] (see their Fig. 5), providing observational constraints on aerosol–cloud interactions in that case.

Figures S2−S5 show the validation of AC for the control simulations of ACAPEX, STEPS, MC3E and GOAmazon cases. The standard errors of observations are used for error bars in all plots and the model line is averaged conditionally with the same conditions as the observations. For ACAPEX, STEPS, MC3E and GOAmazon, more details of the evaluation of AC against ground-based, satellite and other aircraft observations cases are given by Phillips et al. [29], Waman et al. [30, 30], Gupta et al. [31] respectively. In these four prior studies, validation is included for quantities like precipitation rate, vertical velocity statistics, ice concentrations, droplet size and concentrations, liquid water content (LWC), radar reflectivity and hydrometeor size distributions in convective ascent from prescribed aerosol conditions of size, mass loading and chemical composition. All AC simulations are initialized with vertical profiles of loading of each aerosol chemical species, constrained by co-incident ground-based observations (e.g., IMPROVE network) in conjunction with some global model outputs for each location. The same conditional averaging is used for both the simulation and observations.

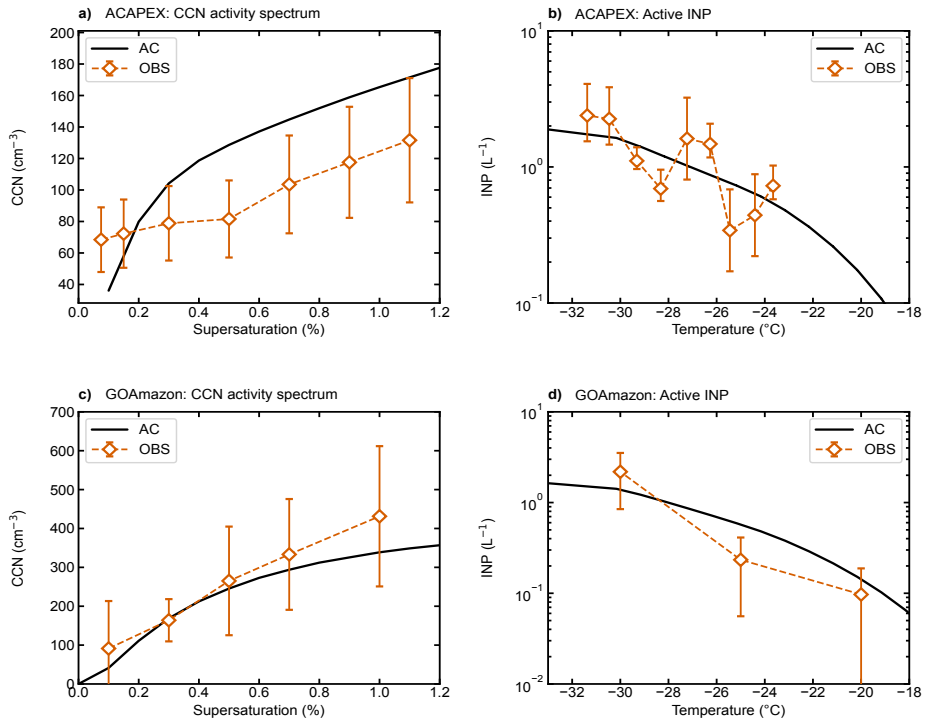


Fig. S1 CCN and INP activity spectra predicted by the AC model (solid) compared with observations (diamonds) for (a, b) the ACAPEX case on 7 Feb 2015 and (c, d) the GOAmazon case on 14 Mar 2014. Panels (a) and (c) show CCN spectra; panels (b) and (d) show INP activity spectra. Observations were made from the research vessel in ACAPEX, near Sacramento, at Manacapuru (Amazonia), and at the ATTO tower in the Amazon. Error bars are standard deviations of samples.

In all validation plots of cloud properties, the aircraft data are from the same time, day and location of the simulation domain. Inevitably, the simulations were idealized in the sense that cloud statistics were predicted, and the precise location of each cloud was not predicted. In Figures S2-S5, the choice of vertical velocity range for conditional averaging reflects the predominant basic cloud type in each case. For example, if the basic cloud type is stratiform, then the choice of condition for averaging $|w|<1$ m/s. In GOAmazon, the aircraft sampled mostly only the stratiform cloud from convective outflow, with little sampling of the cores, which affected the choice of the range of vertical velocities for the conditional averaging.

For stratiform cloud in ACAPEX, the predicted average of the filtered number concentration of ice particles (larger than 200 μm) is consistent with *in-situ* observations, having the same order of magnitude (Fig. S2a). Two long-duration observational samples, each lasting thousands of seconds (at about -10 and -16 °C), bracket the model prediction and dominate the statistics, demonstrating that the AC model accurately captures the representative ice number concentrations in stratiform regions. Corresponding predictions of cloud LWC, mean diameter of cloud-droplets and their number

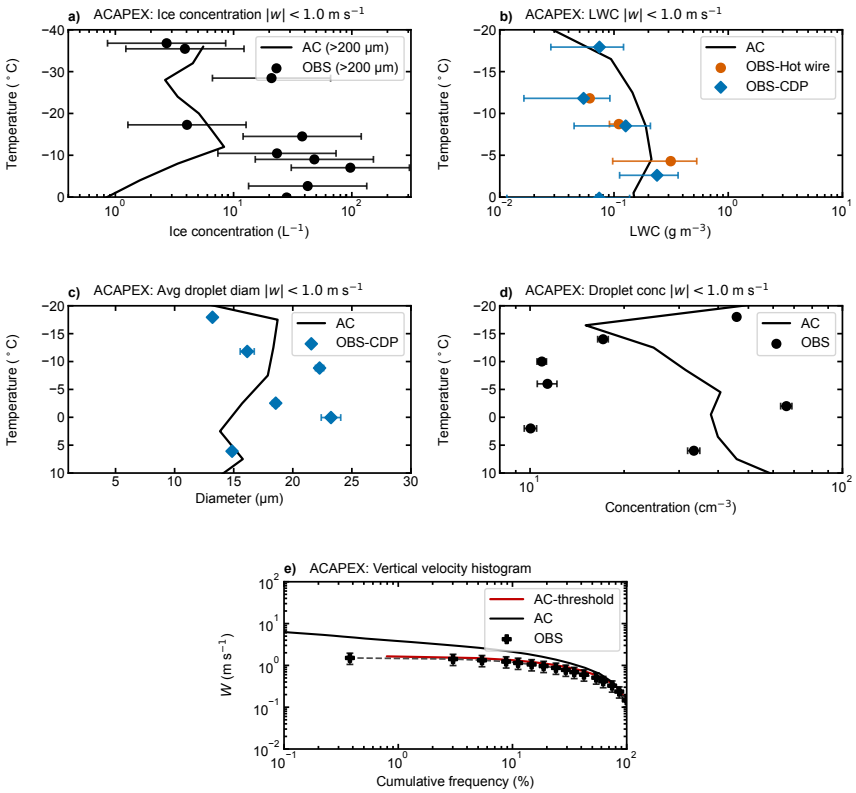


Fig. S2 The validation of the AC simulation for ACAPEX against aircraft observations is shown for predicted (solid black line) and observed (filled symbols) cloud-microphysical properties conditionally averaged over stratiform regions of vertical velocities ($|w| < 1$ m/s), for: (a) concentrations of ice particles >200 μm for all ice microphysical species (cloud-ice, snow, and graupel/hail), with observations from 2D-S probe (range of detection is 25 to 1280 μm); (b) liquid water content (LWC) measured by hot wire probe (filled circles) and CDP (filled diamonds), with different probes relying on different measurement principles and size ranges; and from CDP measurements (c) mean droplet diameter and (d) droplet concentrations. Numbers by each observational point (sample mean) denote total duration (sec) of each sample. Also shown are (e) observed vertical velocity statistics (filled black plus connected by dashed line) compared with AC (solid black line) and with the subset of simulated vertical velocities less than the maximum observed by aircraft ('AC-threshold') (solid red line). The 'AC-threshold' prediction provides the most direct comparison, as it mimics the sampling strategy of flights by being based on only the subset of simulated vertical velocities weaker than the maximum ascent observed. Error-bars are standard errors of samples, except for ice concentrations in (a) (measurement uncertainty from biases of probes is factor of 3).

concentrations all differ by less than 40% from observations (e.g., Hot-wire, Nevzorov, Cloud Droplet Probe [CDP]), (Fig. S2c-d). In Figure S2e, the predicted vertical velocity ('AC-threshold', red curve) differs by less than 10-20% from observations at all cumulative frequencies. In view of the sampling strategy of the aircraft, avoiding any convective ascent, we analysed for this red curve only the subset of simulated vertical velocities weaker than the maximum ascent observed.

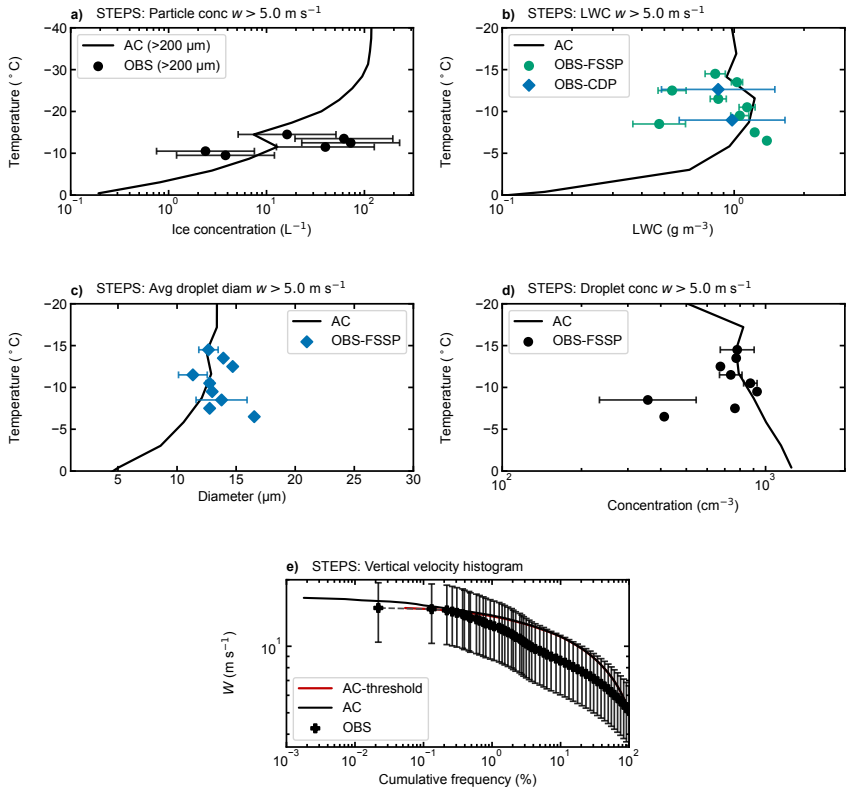


Fig. S3 Evaluation of the AC simulation for STEPS against aircraft data, with predicted (solid black line) and observed (filled symbols) cloud-microphysical properties conditionally averaged over convective updrafts with $w > 5$ m/s: (a) concentrations of ice particles > 0.2 mm, using the 2DC probe data; (b) observed liquid water content (LWC) measured by the FSSP (filled circles) and CDP (filled diamonds); and (c) mean droplet diameter and (d) droplet concentrations, measured by the FSSP. Also shown are (e) vertical velocity statistics, observed (filled black plus mark connected by dashed line) and predicted, both fully (black solid line) and with 'AC-threshold' (solid red line), as in Fig. 3. Error-bars are standard errors of samples yielding plotted means, except for ice concentrations (factor of 3 error).

In the deep convection of STEPS, cloud-bases were cold (about 0 °C). There was sampling of moderate updrafts greater than 5 m/s in the convective cores by the armoured aircraft (T28) [29]. Such ascent is key for large precipitation particles and SIP. Hence, ice number concentrations for particles of maximum dimension greater than 0.2 mm are conditionally averaged over vertical velocities greater than 5 m/s, for the AC control simulation and observations (2DC probe) of STEPS (Figure S3a). The predicted ice concentrations differ by less than about 40% from the observations at all flight levels. Similarly, the predictions for droplet number concentration (Figure S3b), LWC (S3c) and mean droplet diameter (Figure S3d) differ by less than about 30% from observations (CDP, Forward Scattering Spectrometer Probe [FSSP]). For all quantities, predictions lie within the error bars of observations. The observed lack

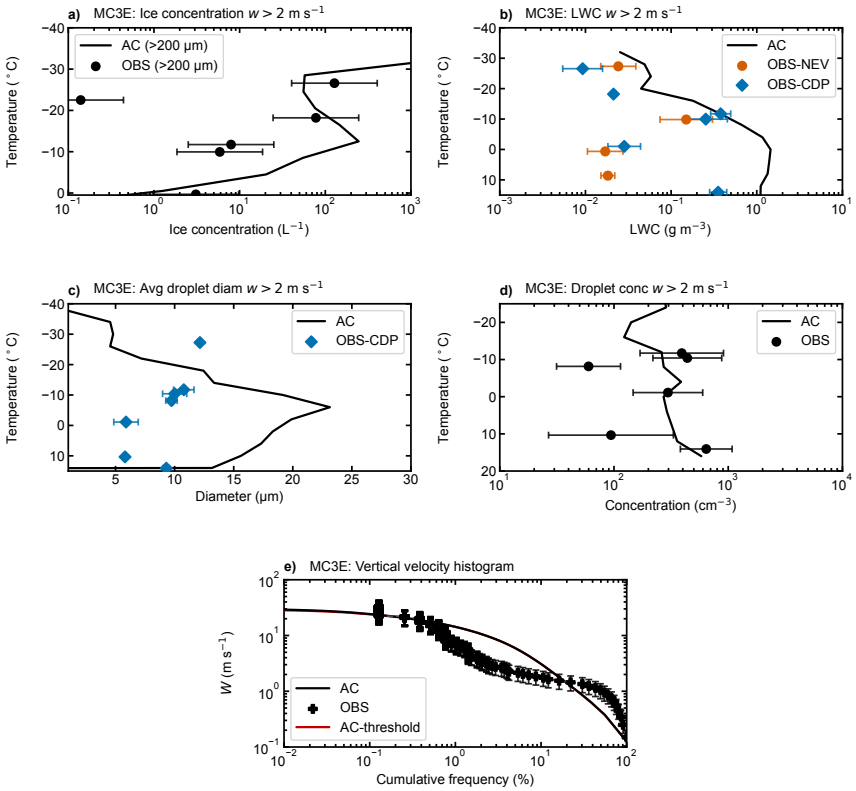


Fig. S4 Evaluation of AC simulation of MC3E case against aircraft data, for microphysical properties conditionally averaged over the convective updrafts for w $>$ 2 m/s, predicted (black solid line) and observed (filled symbols) for: (a) concentrations of ice particles $>$ 0.2 mm compared with observations by HVPS (detecting particles between 150 μm and 19.2 mm); (b) LWC, measured by Nevzorov probe (filled circles, measurement range of 0.005 to 3 g/m^3) and CDP (filled diamonds); (c) mean cloud droplet diameter and (d) cloud droplet concentrations, measured by CDP. Numbers by each observational point denote total duration (sec) of each sample. Also shown are (e) vertical velocity statistics with the observations (filled black plus mark connected by dashed line) and predicted by AC, both fully (black solid line) and with 'AC-threshold' (solid red line), plotted as in Fig. S4. Error-bars are standard errors of samples yielding plotted means, except for ice concentrations (factor of 3 uncertainty is plotted).

of activity of the warm rain process in STEPS, due to the cold continental cloud base, is reproduced by AC, with flights reporting almost no supercooled raindrops [29]. The predicted vertical velocity differs by less than 30% from observations at each frequency (Figure S3e).

For deep convection of MC3E with warmer bases, cloud-microphysical properties predicted by the AC, including mean diameter and number concentrations of cloud-droplets (CDP), ice number concentrations (HVPS) and LWC (Nevzorov probe), all approximately agree with the aircraft observations for convective updrafts (w $>$ 2 m/s), considering all uncertainties in measurements. At levels near -26°C, where

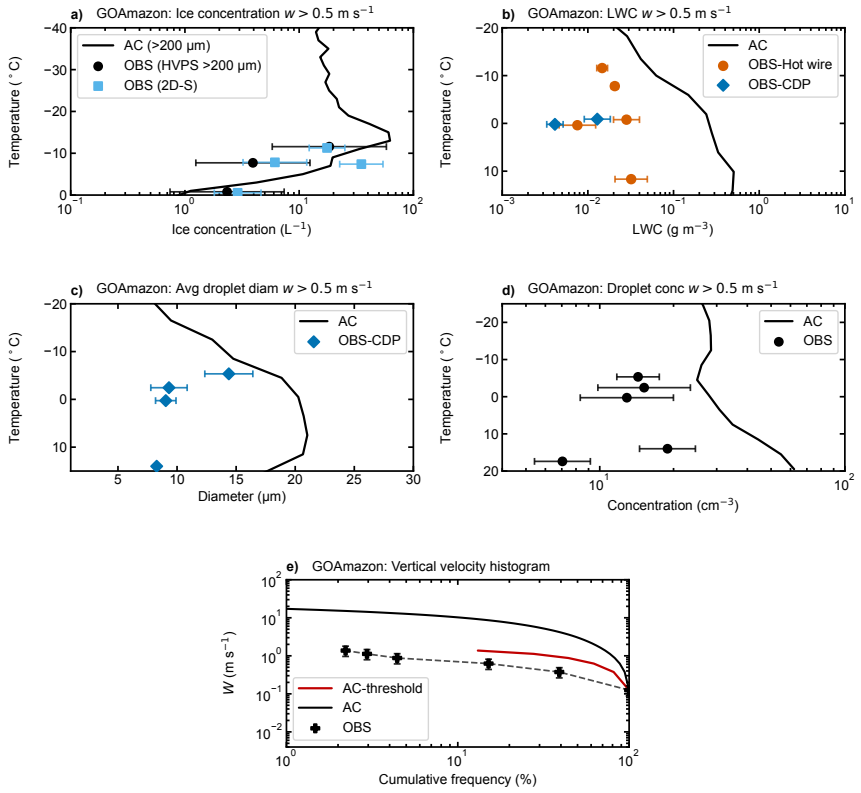


Fig. S5 Same as S4 but for GOAmazon and conditionally averaged over updrafts with w > 0.5 m/s. This lower threshold of ascent, relative to both other convective cases (Fig.S3 S4), was necessitated by the sampling strategy of the aircraft.

about 90% of the sampling occurred, the predicted number concentrations of ice particles (> 0.2 mm) in convective ascent ($w > 2$ m/s) agree with aircraft observations to within about 10% (Figure S4a). In the lower half (0 to about −20 °C) of the mixed-phase region, sampling was scarce and predicted ice concentrations differs from observations by less than the observations differ from each other. Moreover, the predicted droplet size, which in reality determines coalescence and hence the precipitation mechanism, agrees with observations with an error of only 10-40 % (Figure S4c). The predicted vertical velocity by AC differs by less than a factor of 2 from the observations at each frequency (Figure S4e). Again, the observations of vertical velocities reveal non-random sampling by the aircraft and avoidance of moderate convection.

For the very warm-based deep convection of GOAmazon, flights avoided convective cores and only sampled their outflow of stratiform cloud. Hence, the validation focusses on slower updrafts. Predicted cloud droplet properties, such as mean size (Figure S5c) and number concentrations (Figure S5d), agree with aircraft observations (CDP) to within an order of magnitude, averaging over ascent greater than 0.5 m/s. Predicted ice number concentrations (Figure S5a) agree with observations (HVPS) within the

observational uncertainty. This measurement uncertainty is approximately a factor of 3, consistent with estimates from Field et al. [32] and Korolev et al. [33], which account for instrument biases such as artificial shattering, undercounting from large particles obscuring others, classification errors (liquid vs ice), and detection limitations. The GOAmazon HVPS probe included shatter-reduction tips from Korolev et al. [33], which reduce, but do not eliminate, this uncertainty.

In this tropical case, the abundance of warm rain depletes cloud-liquid during lengthy ascent to the freezing level, curbing the supercooled LWC aloft, and the model realistically captures this relative to the observations from the Hot Wire probe and CDP (Figure S5b). Moreover, the predicted vertical velocity agrees, to within a factor of two, with aircraft observations at each frequency, comparing in the range observed (Figure S5e, black dashed and red lines). Also, the simulation shows of up to 20 m/s at a frequency of 1% (Figure S5e, black full line).

S4 Additional results

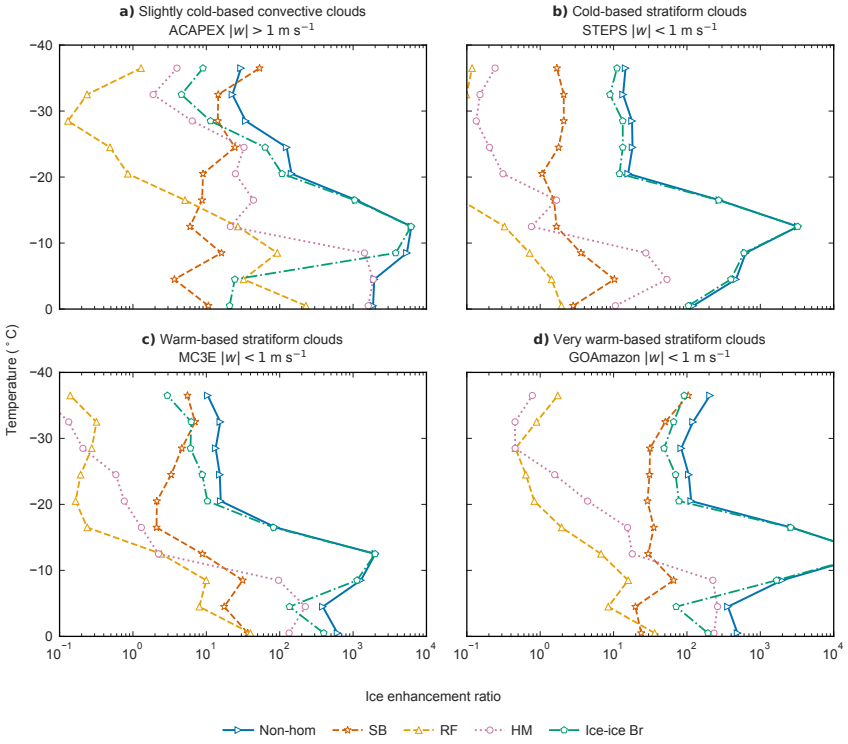


Fig. S6 Vertical profiles of total IE ratio for non-homogeneous ice from all SIP mechanisms (blue right-pointing triangle, "Non hom") are shown, conditionally averaged over convective (a) ACAPEX, and stratiform (b) STEPS, (c) MC3E, and (d) GOAmazon clouds regions for four cases. Also, displayed individual contributions are from the four SIP mechanisms, namely sublimational breakup ('SB'; red stars), raindrop-freezing fragmentation ('RF'; yellow upward-pointing triangles), HM process ('HM'; mauve circles), and ice-ice collisional breakup ('Ice-ice BR'; green pentagon). In these panels, the presented cloud-types are non-dominant.

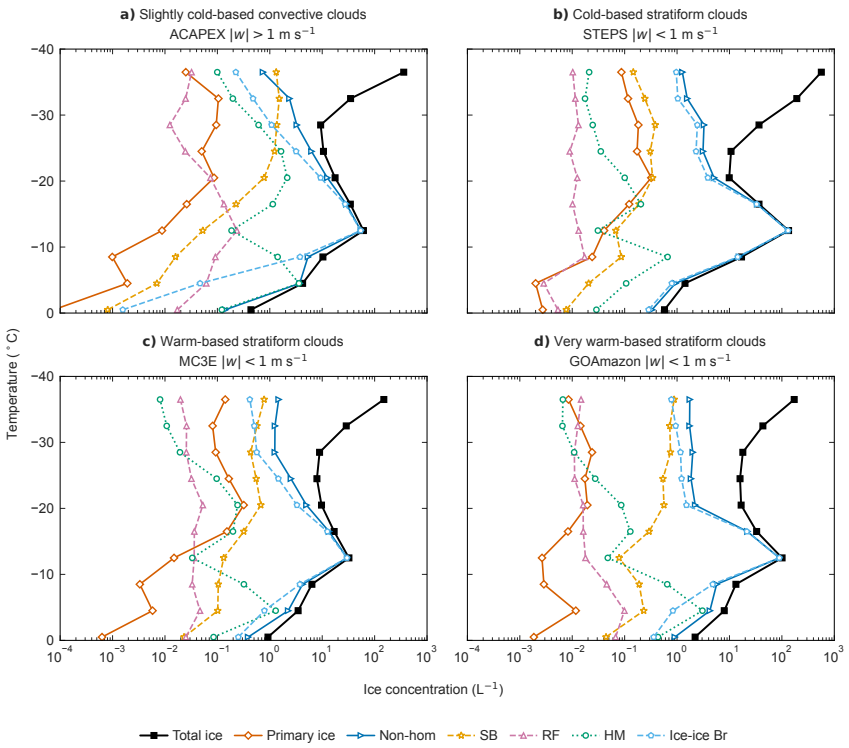


Fig. S7 Vertical profiles of total ice concentrations ('Total ice'; black squares) and their contribution from 'non-homogeneous' ice not initiated by homogeneous freezing ('Non-hom'; blue right-pointing triangles) and primary ice ('Primary ice'; crimson diamonds) are displayed, conditionally averaged over convective (a) ACAPEX, and stratiform (b) STEPS, (c) MC3E, and (d) GOAmazon clouds regions for these four cases. Also, individual SIP mechanisms contributions are also displayed here-similar to Figure S6.

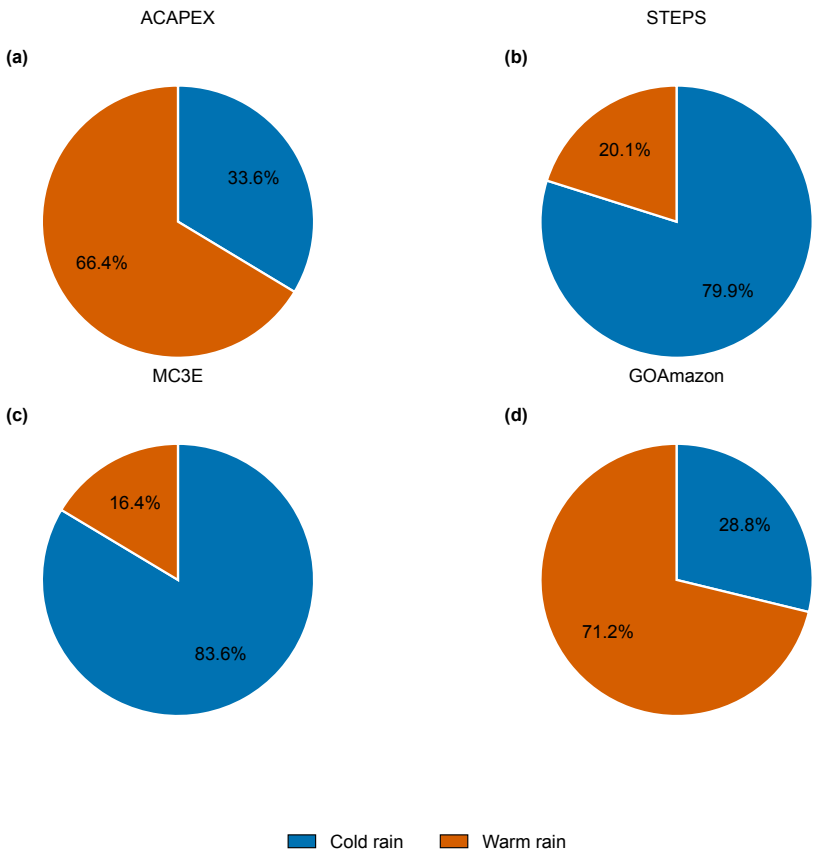


Fig. S8 Total contribution of warm rain (vermillion) or cold (blue) rain is displayed for (a) ACAPEX, (b) STEPS, (c) MC3E and (d) GOAmazon.

References

[1] Hobbs, P.V.: Ice multiplication in clouds. Journal of the Atmospheric Sciences **26**, 315–318 (1969) https://doi.org/10.1175/1520-0469(1969)026⟨0315:IMIC⟩2.0.CO;2

[2] Hobbs, P.V., Stith, J.L., Radke, L.F.: Cloud-active nuclei from coal-fired electric power plants and their interactions with clouds. Journal of Applied Meteorology **19**, 439–451 (1980) https://doi.org/10.1175/1520-0450(1980)019⟨0439:CANFCF⟩2.0.CO;2

[3] Pruppacher, H.R., Klett, J.D.: Microphysics of clouds and precipitation. Kluwer Academic Publishers, Amsterdam1997 (1997)

[4] Hallett, J., Mossop, S.C.: Production of secondary ice particles during the riming

process. Nature **249**, 26–28 (1974) https://doi.org/10.1038/249026a0

[5] Phillips, V.T.J., Patade, S., Gutierrez, J., Bansemer, A.: Secondary ice production by fragmentation of freezing drops: Formulation and theory. Journal of the Atmospheric Sciences **75**, 3031–3070 (2018) https://doi.org/10.1175/JAS-D-17-0190.1

[6] Deshmukh, A., Phillips, V.T.J., Bansemer, A., Patade, S., Waman, D.: New empirical formulation for the sublimational breakup of graupel and dendritic snow. Journal of the Atmospheric Sciences **79**, 317–336 (2022) https://doi.org/10.1175/JAS-D-20-0275.1

[7] Vardiman, L.: The generation of secondary ice particles in clouds by crystal–crystal collision. Journal of the Atmospheric Sciences **35**, 2168–2180 (1978) https://doi.org/10.1175/1520-0469(1978)035⟨2168:TGOSIP⟩2.0.CO;2

[8] Fridlind, A.M., Ackerman, A.S., McFarquhar, G., Zhang, G., Poellot, M.R., DeMott, P.J., Prenni, A.J., Heymsfield, A.J.: Ice properties of single-layer stratocumulus during the mixed-phase arctic cloud experiment: 2. model results. Journal of Geophysical Research: Atmospheres **112** (2007) https://doi.org/10.1029/2007JD008646

[9] Yano, J.I., Phillips, V.T.J.: Ice-ice collisions: An ice multiplication process in atmospheric clouds. Journal of the Atmospheric Sciences **68**, 322–333 (2011) https://doi.org/10.1175/2010JAS3607.1

[10] Phillips, V.T.J., Yano, J.I., Khain, A.: Ice multiplication by breakup in ice–ice collisions. part i: Theoretical formulation. Journal of the Atmospheric Sciences **74**, 1705–1719 (2017) https://doi.org/10.1175/JAS-D-16-0224.1

[11] Takahashi, T., Nagao, Y.: Possible high ice particle production during graupel-graupel collisions. Journal of the atmospheric sciences **52**(24) (1995)

[12] Gautam, M., Waman, D., Patade, S., Deshmukh, A., Phillips, V., Jackowicz-Korczynski, M., Paul, F.P., Smith, P., Bansemer, A.: Fragmentation in collisions of snow with graupel/hail: New formulation from field observations. Journal of the Atmospheric Sciences **81**(12), 2149–2164 (2024)

[13] Johnson, D.A., Hallett, J.: Freezing and shattering of supercooled water drops. Quarterly Journal of the Royal Meteorological Society **94**, 468–482 (1968) https://doi.org/10.1002/qj.49709440204

[14] Brownscombe, J.L., Goldsmith, P.: On the possible production of submicron ice fragments during riming or the freezing of droplets in free fall. In: Preprints, International Cloud Physics Conference, pp. 27–28. Royal Meteorological Society, London, United Kingdom (1972)

[15] Pruppacher, H.R., Schlamp, R.J.: A wind tunnel investigation of ice multiplication by freezing of waterdrops falling at terminal velocity in air. Journal of Geophysical Research **80**, 380–386 (1975) https://doi.org/10.1029/JC080i003p00380

[16] Takahashi, C., Yamashita, A.: Production of ice splinters by the freezing of water drops in free fall. Journal of the Meteorological Society of Japan **55**, 139–141 (1977) https://doi.org/10.2151/jmsj1965.55.1_139

[17] Schaefer, V.J., Cheng, R.J.: The production of ice crystal fragments by sublimation and electrification. Journal de Recherches Atmosphériques **5**, 5–10 (1971)

[18] Oraltay, R.G., Hallett, J.: Evaporation and melting of ice crystals: A laboratory study. Atmospheric Research **24**, 169–189 (1989) https://doi.org/10.1016/0169-8095(89)90044-6

[19] Bacon, N.J., Swanson, B.D., Baker, M.B., Davis, E.J.: Breakup of levitated frost particles. Journal of Geophysical Research: Atmospheres **103**, 13763–13775 (1998) https://doi.org/10.1029/98JD01162

[20] Dong, Y., Oraltay, R.G., Hallett, J.: Ice particle generation during evaporation. Atmospheric Research **32**(1), 45–53 (1994) https://doi.org/10.1016/0169-8095(94)90050-7

[21] Chin, M., Rood, R.B., Lin, S.-J., Müller, J.-F., Thompson, A.M.: Atmospheric sulfur cycle simulated in the global model gocart: Model description and global properties. Journal of Geophysical Research: Atmospheres **105**(D20), 24671–24687 (2000)

[22] Phillips, V.T.J., DeMott, P.J., Andronache, C., Pratt, K.A., Prather, K.A., Subramanian, R., Twohy, C.: Improvements to an empirical parameterization of heterogeneous ice nucleation and its comparison with observations. Journal of the Atmospheric Sciences **70**, 378–409 (2013) https://doi.org/10.1175/JAS-D-12-080.1

[23] Waman, D., Deshmukh, A., Jadav, A., Patade, S., Gautam, M., Phillips, V.T.J., Bansemer, A., Jakobsson, J.: Effects from time dependence of ice nucleus activity for contrasting cloud types. Journal of the Atmospheric Sciences **80**, 2013–2039 (2023)

[24] Andreae, M.O., *et al.*: Carbon monoxide and related trace gases and aerosols over the amazon basin during the wet and dry seasons. Atmospheric Chemistry and Physics **12**, 6041–6065 (2012) https://doi.org/10.5194/acp-12-6041-2012

[25] Andreae, M.O., *et al.*: The amazon tall tower observatory (atto): Overview of pilot measurements on ecosystem ecology, meteorology, trace gases, and aerosols. Atmospheric Chemistry and Physics **15**, 10723–10776 (2015) https://doi.org/10.

5194/acp-15-10723-2015

[26] Martin, S.T., *et al.*: The green ocean amazon experiment (goamazon2014/5) observes pollution affecting gases, aerosols, clouds, and rainfall over the rain forest. Bulletin of the American Meteorological Society **98**, 981–997 (2017) https://doi.org/10.1175/BAMS-D-15-00221.1

[27] Levin, E.J., DeMott, P.J., Suski, K.J., Boose, Y., Hill, T.C., McCluskey, C.S., Schill, G.P., Rocci, K., Al-Mashat, H., Kristensen, L.J., *et al.*: Characteristics of ice nucleating particles in and around california winter storms. Journal of Geophysical Research: Atmospheres **124**(21), 11530–11551 (2019)

[28] Schrod, J., Thomson, E.S., Weber, D., Kossmann, J., Pöhlker, C., Saturno, J., Ditas, F., Artaxo, P., Clouard, V., Saurel, J.M., Ebert, M., Curtius, J., Bingemer, H.G.: Long-term deposition and condensation ice-nucleating particle measurements from four stations across the globe. Atmospheric Chemistry and Physics **20**(24), 15983–16006 (2020)

[29] Phillips, V.T.J., *et al.*: Ice multiplication by breakup in ice–ice collisions. part ii: Numerical simulations. Journal of the Atmospheric Sciences **74**, 2789–2811 (2017) https://doi.org/10.1175/JAS-D-16-0223.1

[30] Waman, D., Patade, S., Jadav, A., Deshmukh, A., Gupta, A.K., Phillips, V.T.J., Bansemer, A., DeMott, P.J.: Dependencies of four mechanisms of secondary ice production on cloud-top temperature in a continental convective storm. Journal of the Atmospheric Sciences **79**, 3375–3404 (2022) https://doi.org/10.1175/JAS-D-21-0278.1

[31] Gupta, A.K., Deshmukh, A., Waman, D., Patade, S., Jadav, A., Phillips, V.T., Bansemer, A., Martins, J.A., Gonçalves, F.L.: The microphysics of the warm-rain and ice crystal processes of precipitation in simulated continental convective storms. Communications Earth & Environment **4**, 226 (2023)

[32] Field, P.R., Möhler, O., Connolly, P., Krämer, M., Cotton, R., Heymsfield, A.J., Saathoff, H., Schnaiter, M.: Some ice nucleation characteristics of asian and saharan desert dust. Atmospheric Chemistry and Physics **6**, 2991–3006 (2006) https://doi.org/10.5194/acp-6-2991-2006

[33] Korolev, A., Emery, E., Strapp, J., Cober, S., Isaac, G., Wasey, M., Marcotte, D.: Small ice particles in tropospheric clouds: Fact or artifact? airborne icing instrumentation evaluation experiment. Bulletin of the American Meteorological Society **92**, 967–973 (2011) https://doi.org/10.1175/2010BAMS3141.1